Biosensors and Bioelectronics 151 (2020) 111976

Contents lists available at ScienceDirect

Biosensors and Bioelectronics

journal homepage: http://www.elsevier.com/locate/bios

Photoelectrochemical detection of circulating tumor cells based on aptamer conjugated Cu_2O as signal probe

Junjun Luo, Dong Liang, Dan Zhao, Minghui Yang *

Key Laboratory of Hunan Province for Water Environment and Agriculture Product Safety, College of Chemistry and Chemical Engineering, Central South University, Changsha, 410083, China

ARTICLE INFO

Keywords:
Photoelectrochemical
Hexagonal carbon nitride tubes
Circulating tumor cells
Magnetic nanospheres
Antiepithelial cell adhesion molecule

ABSTRACT

In this work, a sensitive and reliable photoelectrochemical (PEC) biosensor was proposed based on hexagonal carbon nitride tubes (HCNT) as photoactive material for detection of circulating tumor cells (CTCs). Magnetic Fe_3O_4 nanospheres (MNs) and Cu_2O nanoparticles (Cu_2O NPs) were utilized for highly efficient magnetic capture of CTCs and for signal amplification, respectively. First, anti-epithelial cell adhesion molecule (EpCAM) antibody was linked onto MNs for capture and enrichment of CTCs. With the captured MCF-7 coated onto the electrode, the photocurrent intensity of HCNT was decreased due to the steric hindrance derived from MCF-7. Then, when the Cu_2O-aptamer probe was bound onto the CTC surface, the photocurrent intensity was further decreased because Cu_2O NPs competed with HCNT for absorption of exciting light and the aptamer molecules increased the steric hindrance, which leads to significantly decreased photocurrent response, thus realizing dual signal amplification. Using the breast cancer cell MCF-7 as a model, the proposed PEC biosensor displays good performances with a linear range from 3 to 3000 cell mL^{-1} and limit of detection down to 1 cell mL^{-1}. The HCNT-based PEC biosensor shows good performance for detection of CTCs, which may have potential applications in cancer diagnostics and therapeutics.

1. Introduction

Circulating tumor cells (CTCs) are cancer cells that break away from a primary tumor site and circulate in the peripheral blood to form secondary tumor in human body, which act as the cellular origin of cancer metastases (Miao and Tang, 2019; Ouyang et al., 2015; Zheng et al., 2014a). As a "tumor liquid biopsy", CTC quantification plays a vital role in evaluating cancer dissemination, predicting patient prognosis and also the assessment of therapeutic treatments. CTC detection acts as a reliable potential alternative to invasive biopsies (Wu et al., 2014). However, identifying CTCs in blood samples is difficult due to the extremely low abundance (a few to hundreds per milliliter) of CTCs among a large number (10^9 mL^{-1}) of hematologic cells (Huang et al., 2014; Lin et al., 2014; Wen et al., 2014). Hence, it is highly imperative to develop a feasible platform for sensitive detection of CTCs. Diverse techniques have been established for CTCs detection, such as the fluorescence spectroscopy (Hua et al., 2013), differential pulse voltammetry (DPV) (Yang et al., 2018b), electrochemiluminescence (ECL) (Motaghi et al., 2018), electrochemical impedance spectroscopy (EIS)(Yan et al., 2019), and microcantilevers (Li et al., 2019). However, these strategies suffer from several weaknesses, mainly low sensitivity, which ultimately go against their application in clinical diagnosis. Thus, new techniques with improved sensitivity and simple detection procedures are still highly required.

Photoelectrochemical (PEC) biosensor, as one of the most promising and dynamically developing analytical technologies, has received great attention due to its desirable analytical performance, especially its high sensitivity (Yang et al., 2018a). The high sensitivity originates from its complete separation of the light excitation source and photocurrent detection signal, which is conducive to reduce the undesired background noise (Li et al., 2018b). What's more, the PEC instrument is simple and easy to miniaturize since it smartly integrates the photoexcitation process with electrochemical bioanalysis (Jiang et al., 2017). The performance of PEC biosensor largely relies on the photo-to-current conversion efficiency of photoactive materials used in the biosensor. Traditionally, metal oxide semiconductors and metal sulfide are the most popular photoactive materials applied in PEC biosensing platforms. Nevertheless, the practical applications of these photoactive materials are limited by their wide band gap property or photocorrosion effect, which result in poor utilization of light and low system stability

* Corresponding author.
E-mail address: yangminghui@csu.edu.cn (M. Yang).

https://doi.org/10.1016/j.bios.2019.111976
Received 18 October 2019; Received in revised form 13 December 2019; Accepted 17 December 2019
Available online 20 December 2019

(Fan et al., 2016; Hu et al., 2020; Peng et al., 2018; Qiu et al., 2018). Besides, the presence of heavy metals may leads to the cytotoxicity (Li et al., 2018b). Moreover, high energy photons produced by ultraviolet light might affect the activity of biomolecular and performance of the biosensor.

To overcome the aforementioned concerns, many researches have paid attention to develop innovative and powerful photoactive materials. Graphitic carbon nitride (g-C_3N_4), as a metal-free and earth-abundant photocatalytic material, has attracted considerable interest due to its unique properties, such as low cost, high stability, non-toxicity, narrow band gap (~2.7 eV) and visible-light response (Hu et al., 2019; Li et al., 2017a). Nevertheless, in bulk g-C_3N_4, the photo-excited charge carriers are apt to transfer in the basal plane instead of the interlayers due to the large electrostatic potential barrier perpendicular to the basal plane, which goes against the rule of separation of photoinduced electrons and holes (Tian et al., 2019). To solve this problem, recently, a phosphorus-doped hexagonal tubular carbon nitride (P-TCN) was prepared through a phosphorus acid-aided hydrothermal process and thermal treatment (Guo et al., 2016). Besides, a boron-doped graphitic carbon nitride hollow tube (BCNT) was synthesized by a facile hydrothermal and heat treatment method (Wang et al., 2018). Cuprous oxide (Cu_2O), a p-type semiconductor with a narrow band gap of about 2.0 eV, is a promising material due to its environmental compatibility, non-toxicity and earth abundance (Li et al., 2017b). Recently, Cu_2O nanoparticles (Cu_2O NPs) have exhibited potential applications in the fields of photocatalysis (Kim et al., 2018; Zeng et al., 2019), electrocatalysis (Ji et al., 2017; Song et al., 2019), photodetectors (Ghamgosar et al., 2018; Kallatt et al., 2018), water splitting (Shyamal et al., 2019; Wei et al., 2017; Wu et al., 2018), solar cells (Musselman et al., 2012), supercapacitors (Asen and Shahrokhian, 2017; Wang et al., 2015), lithium ion batteries (Goyal et al., 2011; Xu et al., 2015), biosensors (Khan et al., 2014; Lv et al., 2017) and gas sensing (Zhang et al., 2006), due to favorable electrical, optical, and super ionic properties. Thus, Cu_2O has a great potential for practical applications in PEC biosensor.

In this work, a sensitive and reliable hexagonal carbon nitride tubes (HCNT) based PEC biosensor was proposed for CTCs detection by integrating magnetic Fe_3O_4 nanospheres (MNs) for enrichment as well as isolation of CTCs and Cu_2O-aptamer for amplifying the detection response (Scheme 1). The breast cancer tumor cell MCF-7 was used as a model. MCF-7 cells from peripheral blood were enriched and isolated by anti-EpCAM-MNs nanocomposite because of the specific binding of the anti-EpCAM with EpCAM on the surfaces of MCF-7 cells. With the captured MCF-7 coated onto the electrode, the photocurrent intensity of HCNT was decreased due to the steric hindrance derived from MCF-7. Thereafter, Cu_2O-aptamer probe was linked onto the MCF-7 cell through the specific binding of the aptamer with MUC1 that was over-expressed on the MCF-7 cell surface. Then, the photocurrent intensity of HCNT was sharply decreased because Cu_2O NPs would competitively absorb the exciting light, thus amplifying the detection response. In addition, aptamer molecules can increase the steric hindrance of the working electrode, hampering the electron delivery and further leading to decrease of the response signal. In this study, the photocurrent intensity decrease is proportional to the content of the CTCs. Accordingly, a HCNT-based PEC biosensor was successfully established for detection of CTCs.

2. Experimental section

2.1. Materials and apparatus

The 5′-thiol modified MCF-7 binding aptamer was synthesized and purified by Sangon Biotechnology Co. Ltd. (Shanghai, China), which had a sequence as 5′-SH- CACTACAGAGGTTGCGTCTGTCCCACGTTG TCATGGGGGGTTGGCCTG-3′. Ethylene glycol (EG) and antiepithelial cell adhesion molecule antibody (anti-EpCAM) were obtained from Abcam Co., Ltd. (Cambridge, MA). N-(3-dimethylamminopropyl)-N′-ethylcarbodiimide hydrochloride (EDC), N-hydroxysuccinimide (NHS), bovine serum albumin (BSA), phosphate buffered saline (PBS), poly (acrylic acid) (PAA), iron trichloride hexahydrate ($FeCl_3{\cdot}6H_2O$), tris(2-chloro-2-ethyl)phosphate (TCEP), copper (II) chloride dihydrate ($CuCl_2{\cdot}2H_2O$) and melamine were purchased from Sigma-Aldrich. Sodium acetate anhydrous (NaAc), ascorbic acid (AA) and sodium dodecyl sulfate (SDS) were supplied from Sinopharm Chemical Reagent Co., Ltd (Shanghai, China). Human serum samples were received from the Xiangya hospital (Changsha, China). All other reagents were of analytical grade and used without further purification. Ultrapure water (18.2 MΩ cm resistivity at 25 °C, Millier Q) was used in all experiments.

The crystal phases of materials were investigated by X-ray diffraction (XRD) on a DX-2700 diffractometer using Cu-Ka radiation under 40 kV

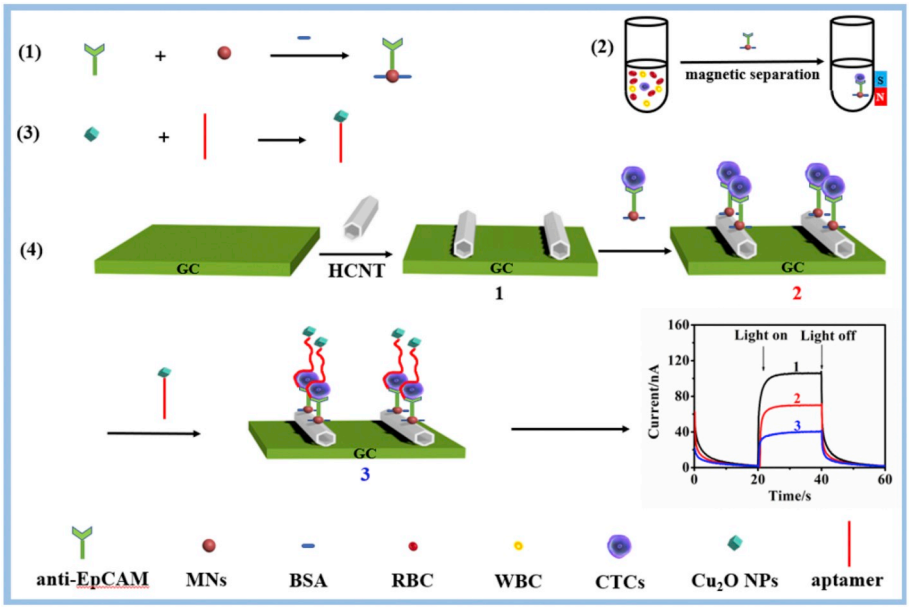

Scheme 1. Schematic representation of CTC measurement in whole blood based on MNs isolation of CTCs and Cu_2O-aptamer as signal probe: (1) Preparation of Anti-EpCAM-MNs nanocomposite; (2) Enrichment and isolation of CTCs; (3) Preparation of Cu_2O-aptamer Probe; (4) PEC Detection of CTCs.

and 30 mA. Transmission electron microscopy (TEM) images were obtained using a JEOL JEM 2010 F electron microscope instrument operating at 200 kV. The micromorphology and elemental composition information of the material were conducted by the scanning electron microscopy (SEM, JEOL, JSM-7800 F). The UV–visible diffuse reflectance spectra (DRS) were collected on a UV–vis spectrophotometer (Shimadzu, UV-2550). The hydrodynamic diameter and zeta potential were determined by Zeta-sizer Nano ZS (Malvern Inc., UK). PEC measurements were conducted by a homemade PEC system equipped with a 500 W Xe lamp with an emission wavelength of 420 nm. Photocurrent was carried out with a CHI 650D electrochemical workstation (China) using glassy carbon electrode with a geometrical circular area (GCE, 5.0 mm in diameter) as the working electrode, a Pt wire as an auxiliary electrode and a saturated Ag/AgCl electrode used as a reference electrode. Cyclic voltammetry (CV) and electrochemical impedance spectroscopy (EIS) were tested in 5 mM $[Fe(CN)_6]^{3-/4-}$ solution containing 0.1 M KCl.

2.2. Synthesis of MNs and preparation of anti-EpCAM-MNs nanocomposite

Carboxyl group-terminated Fe_3O_4 MNs was synthesized according to previously reported hydrothermal method (Zheng et al., 2014b). Briefly, 1.35 g $FeCl_3{\cdot}6H_2O$, 3.2 g NaAc, and 0.5 mL PAA were mixed with 38 mL of ethylene glycol (EG) and then ultrasound at room temperature. Subsequently, the mixture was transferred into a sealed poly-tetrafluoroethylene reaction kettle and maintained at 473 K for 6 h. The black products were obtained by magnetic separation and washed with water and ethanol alternately several times, and finally dried at 343 K in a vacuum drying oven.

Before preparation of anti-EpCAM-MNs nanocomposite, 7.5 mg MN were dissolved in 1.5 mL PBS (0.01 M, pH 6.8) with 75 mM EDC and 75 mM NHS. The mixture was gently shaken at room temperature for 30 min. After carboxyl group of MNs was activated, the MNs was washed three times with 0.01 M PBS (pH 7.2) and then dispersed into 1 mL of PBS (0.01 M, pH 7.2). Under slight stirring, 300 μg anti-EpCAM was added into the solution and incubated for 4 h at room temperature. Then, the MNs were washed three times with water to remove the unbonded anti-EpCAM. The non-specific sites on MNs were blocked using 1% BSA solution for 30 min at room temperature. The obtained anti-EpCAM-MNs nanocomposite was stored at 4 °C for further use.

2.3. Synthesis of Cu_2O NPs and preparation of Cu_2O-aptamer probe

The Cu_2O NPs was prepared according to the previous reports (Li et al., 2017b). Typically, 1 mL $CuCl_2{\cdot}2H_2O$ (1 M) and 0.4 mL SDS (50 mg mL^{-1}) were mixed with 239.6 mL water. Subsequently, 4 mL NaOH (0.5 M) was added into the mixture under magnetic stirring for 30 min. Then, 5 mL AA (0.2 M) was added into the above suspension. After further stirring for 30 min, a brick red dispersion was formed. The resulting precipitate was collected, washed with ethanol and water for three times and dried under vacuum.

The Cu_2O-aptamer probe was prepared according to the previous report with a minor modification (He et al., 2018). Briefly, 2 mg of Cu_2O powder was suspended in 10 mL of PBS containing Tween-20 (0.01 M, 0.1% Tween-20, pH 7.0). The solution was sonicated for about 1 h to obtain the Cu_2O NPs colloid. Prior to use, 300 μL of thiolated MCF-7 aptamer (2 μM) was incubated with 30 μL of TCEP (10 mM) for 30 min to reduce disulfide bonds. Then, 300 μL of the Cu_2O NPs colloid was mixed with the above MCF-7 aptamer, and the solution was incubated on a mixer for 12 h at room temperature. Subsequently, sodium chloride (2 M) was added to the mixture until final concentration of 0.1 M. After 24 h of shaken, the Cu_2O-aptamer probe was centrifugated and washed to remove excess aptamer. Finally, the probe was resuspended in 600 μL water for further use.

2.4. Cell culture and treatment

The MCF-7 and HeLa were cultured in a cell culture flask containing Dulbecco's modified Eagle's medium (DMEM) supplemented with 10% fetal bovine serum, 100 U mL^{-1} penicillin, and 100 μg mL^{-1} streptomycin at 37 °C in a humidified atmosphere containing 5% CO_2. When the cells grew for 2 days, the cells were collected and separated from the medium by centrifugation at 1000 rpm for 5 min. Then, the cells were washed three times with saline solution (0.9% NaCl). The cell sediment was resuspended in saline solution to obtain a homogeneous suspension. The concentration of the cell suspension was determined using a Petroff-Hausser cell counting chamber.

2.5. Capture of MCF-7

For capture and enrichment of cells, anti-EpCAM-MNs nanocomposite (100 μL, 100 μg mL^{-1}) were added into 900 μL MCF-7 cell solution with different concentrations of MCF-7. The mixture was incubated with gentle shaking for 1 h at room temperature. The MNs were isolated and washed with magnetic separation, and then stored at 4 °C. Hela cells were incubated with anti-EpCAM-MNs nanocomposite as a negative control.

2.6. Construction of the PEC biosensor

Prior to modification, 0.05 μm alumina powder was utilized for burnishing the bare GCE followed by ultrasonically washing with ethanol and water several times. Initially, 1 mg of HCNT powder was dispersed into 1 mL of water (including 5 μL Nafion) under sonication for 1 h. Then, 30 μL of the solution was dropped onto the surface of GCE electrode, dried at 37 °C, and thoroughly rinsed with water.

For MCF-7 detection, 30 μL of the MNs with captured MCF-7 was dropped onto electrode surface and incubated for 50 min at 37 °C. Then, 30 μL Cu_2O-aptamer probe (0.2 μg mL^{-1}) was added to electrode surface at 37 °C for 1 h. Finally, electrode surface was thoroughly rinsed before PEC measurements.

2.7. Blood sample analysis

Fresh human whole blood of healthy people was obtained from the Second Xiangya hospital (Changsha, China). The probes of anti-EpCAM-MNs nanocomposite (100 μg mL^{-1}, 100 μL) was added into 900 μL of whole blood spiked with different numbers of MCF-7 cells, followed by gentle stirring for 1 h at 37 °C. Then, the target MCF-7 cells were separated from the above mixture with an external magnet and washed three times using saline solution.

2.8. PEC detection

PEC response of the biosensor was recorded in 1 mM Na_2SO_4 at a bias potential of +0.1 V (vs SCE) under visible light irradiation ($\lambda > 420$ nm).

3. Results and discussion

3.1. Characterization of HCNT

HCNT as photoactive material were synthesized by a hydrothermal method according to our previous work (Luo et al., 2019). The HCNT was characterized by SEM. From Fig. 1A, it can be seen HCNT presents a hexagonal tube structure. Besides, the HCNT show narrow optical absorption at UV–vis region, which is in accordance with our previous work (Fig. 2A).

3.2. Characterization of MNs and anti-EpCAM-MNs nanocomposite

Carboxyl group-terminated Fe_3O_4 MNs were also synthesized using

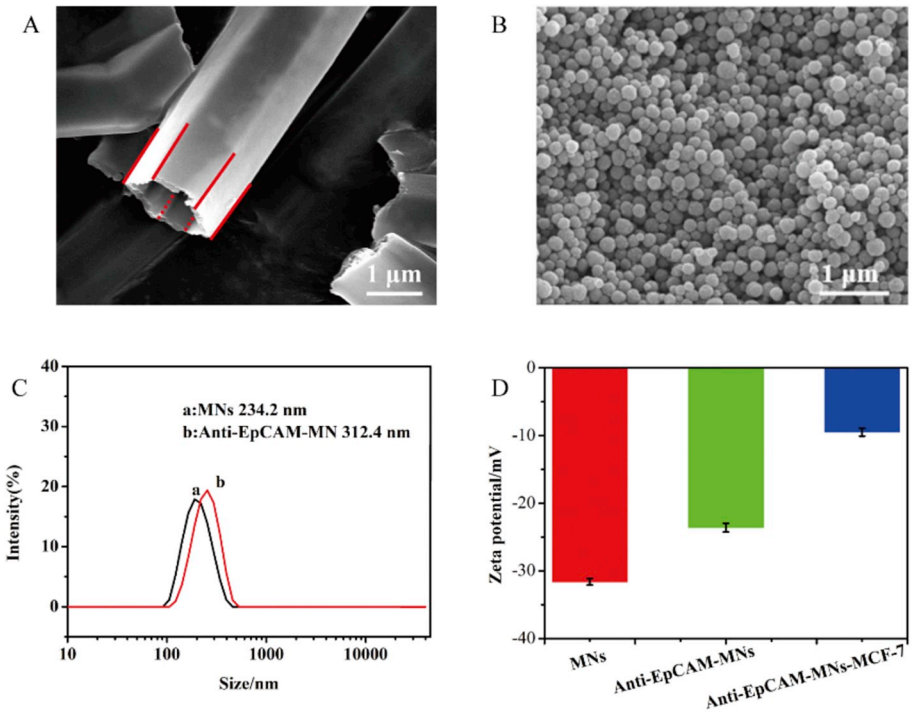

Fig. 1. (A) SEM image of HCNT. (B) SEM image of MNs. (C) Particle size distribution of MNs and anti-EpCAM-MNs nanocomposite. (D) Change of zeta-potential during the modification of the anti-EpCAM-MNs nanocomposite.

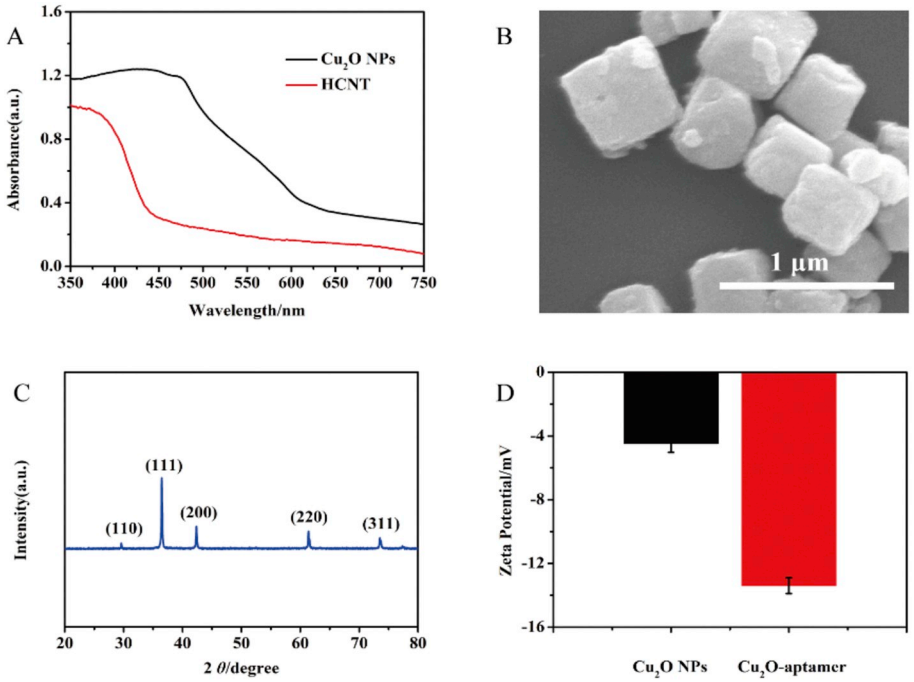

Fig. 2. (A) The UV–visible diffuse reflectance spectra of Cu_2O NPs and HCNT. (B) SEM image of Cu_2O NPs. (C) XRD patterns of Cu_2O NPs. (D) Change of zeta-potential after modification of aptamer onto Cu_2O NPs.

hydrothermal method. From Fig. 1B, it can be seen MNs display spherical particles with relatively uniform morphology. The energy dispersive X-ray spectroscopy (EDX) mapping images reveal that Fe and O elements are uniformly distributed in the MNs (Supporting Information, Fig. S1). The transmission electron microscopy (TEM) images of MNs also show uniform and spherical particles (Supporting Information, Fig. S2) (Zheng et al., 2014b). In addition, the HRTEM images of MNs show clear crystal lattice fringes with two kinds of d-spacing of 0.296 nm and 0.485 nm corresponding to the (220) and (111) plane, respectively (Qiu et al., 2016; Wang et al., 2013) (Supporting Information, Fig. S2). The crystalline structure of MNs was further investigated by X-ray diffraction (XRD). All of the characteristic diffraction peaks are indexed to cubic structure of magnetite, which is in accordance with the reported data (JCPDS No. 01-1111)(Liu et al., 2011) (Supporting Information, Fig. S3).

These results indicated that MNs were successfully synthesized. Due to expression of EpCAM on many CTC surface, anti-EpCAM antibodies were immobilized onto MNs for effective capture and enrichment of CTCs from complex matrices. The immobilization of antibodies onto MNs was achieved through linking the amino groups on antibody with carboxylic groups on MNs via coupling agents of EDC and NHS. Compared to characterization by TEM, the size of MNs measured by dynamic light scattering became larger. The reason is that MNs can form hydrated nanospheres in aqueous solution (Shen et al., 2019). The size of anti-EpCAM-MNs nanocomposite was larger than that of bare MNs (Fig. 1C), which indicated successfully conjugation of anti-EpCAM onto MNs. From Fig. 1D, for zeta potential, the negative charges of MNs reduced after modification with anti-EpCAM, which also validated the successful conjugation of anti-EpCAM onto MNs. After the enrichment and separation of MCF-7, the negative charges were further reduced, confirming the successful capture of MCF-7. Besides, the magnetic properties of MNs and their colloid behavior were studied. The magnetic separation of the MNs in blood and saline solution (0.9% NaCl) at different times were studied (Supporting Information, Fig. S4). After 12 s, the MNs were completely separated, demonstrating the good magnetic response of the MNs.

3.3. Characterization of Cu_2O NPs and Cu_2O-aptamer probe

The Cu_2O NPs were characterized by UV–vis diffuse reflectance spectra of Cu_2O, SEM, XRD and dynamic light scattering. From Fig. 2A, Cu_2O NPs show strong optical absorption range from 350 nm to 750 nm, while HCNT present little optical absorption from 450 nm to 750 nm, indicating Cu_2O NPs not only have better light absorption capacity than HCNT but also can compete with HCNT for absorption of light (Li et al., 2018a). As shown in Fig. 2B, Cu_2O NPs have relatively uniform morphologies with cubic structure. Moreover, the crystal structures of the Cu_2O NPs were characterized by powder XRD. As displayed in Fig. 2C, the characteristic diffraction peaks at 29.5°, 36.4°, 42.3°, 61.3°, 73.5° are assigned to (110), (111), (200), (220) and (311) planes of Cu_2O, respectively (Li et al., 2017b). After modification of aptamer onto Cu_2O, as exhibited in Fig. 2D, the zeta-potential of Cu_2O NPs becomes more negative after aptamer modification, which confirms the successful linking of aptamer on Cu_2O NPs.

3.4. Characterization of the PEC biosensor

Prior to characterization of the PEC biosensor, the concentration of HCNT was optimized. As shown in Fig. S5, the photocurrent gradually enhanced with the increase of HCNT (Supporting Information, Fig. S5). Because 1 mg mL^{-1} of HCNT possesses fairly strong photocurrent, thus, 1 mg mL^{-1} of HCNT was used. Then, cyclic voltammetry (CV) and electrochemical impedance spectroscopy (EIS) were used to characterize the step-by-step electrode modification process. Fig. 3A illustrated the CV of different electrodes in 5.0 mM $[Fe(CN)_6]^{3-/4-}$ containing 0.1 M KCl. When HCNT was coated on the electrode, the peak currents of HCNT/GCE (curve b) were lower than that of a bare GCE (curve a), mainly because of low electronic conductivity of HCNT. Then, the current response decreased again when MNs with captured MCF-7 was immobilized onto the HCNT/GCE electrode (curve c). After the resultant electrode was incubated with Cu_2O-aptamer probe, the CV response declined continually (curve d). The reason may be the Cu_2O-aptamer probe retarded the electron transfer at electrode surface.

For EIS spectrum, from Fig. 3B, it can be seen the bare GCE electrode displays an almost straight line (curve a). After coating HCNT onto the GCE electrode, an obvious semicircle appeared (curve b) due to the weak conductivity of the HCNT. When the captured MCF-7 was immobilized onto the electrode surface, the Ret increased again (curves c) because of the generation of an insulating layer, which impeded the access of the redox probe to the electrode surface (Li et al., 2018b). After the electrode was incubated with the Cu_2O-aptamer probe, the Ret further

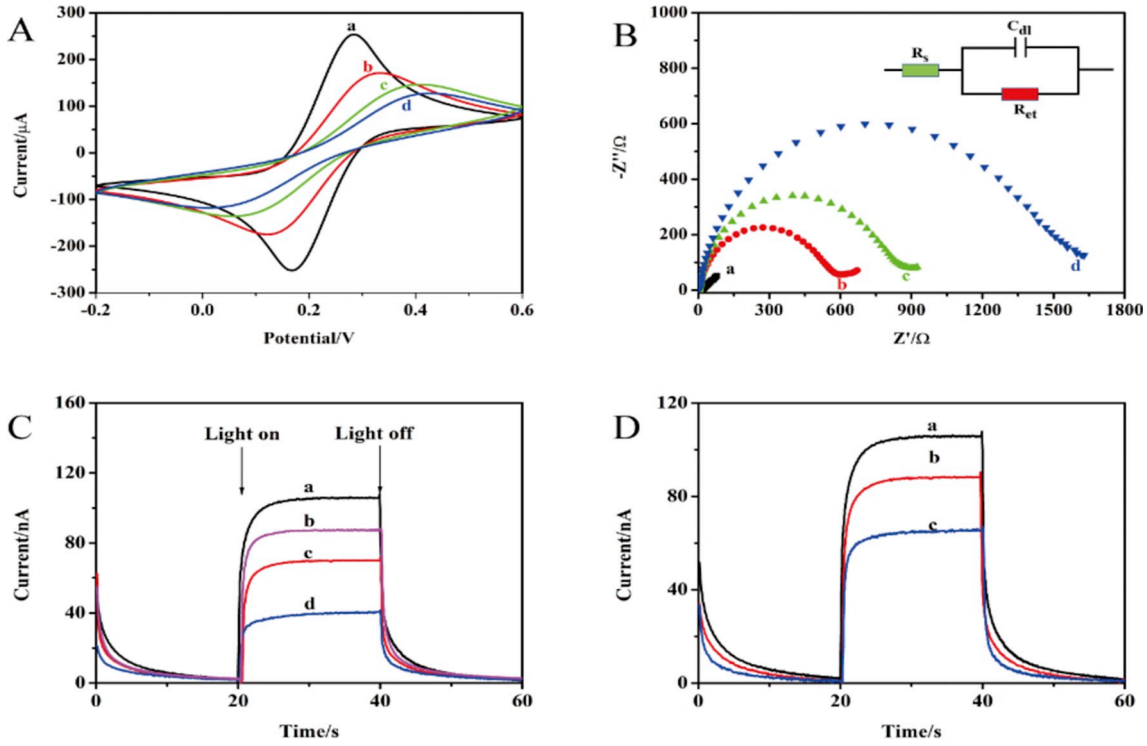

Fig. 3. (A) CV and (B) EIS responses of the PEC biosensor: (a) bare GCE, (b) HCNT/GCE, (c) HCNT/GCE incubated with the captured MCF-7 cells, (d) Biosensor after incubation with 0.2 μg mL^{-1} Cu_2O-aptamer probe. Supporting electrolyte: 5.0 mM $[Fe(CN)_6]^{3-/4-}$ containing 0.1 M KCl.(C) Photocurrent responses of different modified GCE electrodes: (a) HCNT/GCE, (b) HCNT/GCE incubated with the anti-EpCAM-MNs nanocomposite, (c) HCNT/GCE incubated with the MNs captured MCF-7 cells, (d) Biosensor after incubation with 0.2 μg mL^{-1} Cu_2O-aptamer probe. (D) Photocurrent responses of different modified GCE electrodes: (a) HCNT/GCE, (b) after direct incubation with MCF-7, (c) after incubation with 0.2 μg mL^{-1} Cu_2O-aptamer probe.

increased (curves d), proving that the successful fabrication of the PEC biosensor for MCF-7 detection.

To further study the feasibility of the biosensor for CTC detection, the electrode is also characterized by the PEC method. As shown in Fig. 3C, the HCNT/GCE electrode displays high photocurrent response (curve a). After the anti-EpCAM-MNs nanocomposite was immobilized onto HCNT/GCE, the photocurrent intensity reduced because of the steric hindrance of MNs (curve b). When the captured MCF-7 was modified onto the electrode, the photocurrent intensity was further reduced (curve c), which could be ascribed to evident steric hindrance of MCF-7. At last, when the Cu_2O-aptamer probe was specifically bound onto the electrode surface, significant photocurrent decrement was observed (curve d). The reason may be as follows: 1) aptamer molecule with an obvious steric hindrance impeded the electron transfer, leading to reduced photocurrent (Fan et al., 2016; Li et al., 2018a); 2) p-type Cu_2O NPs with a broad absorption range (as shown in Fig. 2A) can competitively absorb the light energy, weakening the light absorption efficiency of HCNT. Besides, the detection of CTCs without MN enrichment was also studied (Fig. 3D). The photocurrent intensity was also reduced when MCF-7 was direct incubation with HCNT/GCE electrode, and then incubation with 0.2 μg mL^{-1} Cu_2O-aptamer probe. These results confirm that the PEC biosensor also has ability to detection CTCs without MN enrichment.

3.5. PEC detection of MCF-7

MCF-7 detection was based on the decrease of photocurrent caused by MCF-7 as well as Cu_2O-aptamer probe. The photocurrent response of the PEC biosensor was directly associated with the concentration of MCF-7. Fig. 4A presents the photocurrent response of the designed PEC biosensor after incubated with different concentrations of MCF-7 and then further incubated with Cu_2O-aptamer probe. With the concentration of MCF-7 elevated, the photocurrent intensity of the biosensor was decreased continually. As displayed in Fig. 4B, the photocurrent response decreased linearly with increasing logarithm of MCF-7 concentration in the range from 3 cell mL^{-1} to 3000 cell mL^{-1}. The limit of detection (LOD, S/N = 3) was calculated to be 1 cell mL^{-1}, which was comparable or even lower than that of previous methods (Supporting Information, Table S1).

3.6. Selectivity, reproducibility, and stability of the PEC biosensor

The performance of the PEC biosensor was assessed by evaluating its selectivity, stability and reproducibility. In order to investigate the selectivity of the PEC biosensor for CTCs, HeLa cells was selected as control since Hela cells do not express EpCAM as well as MUC1 on the cell surface. As shown in Fig. 5A, the photocurrent response to 1000 cell mL^{-1} HeLa is very weak. On the contrary, after 1000 cell mL^{-1} HeLa mixed with different concentrations of MCF-7, the photocurrent intensity is gradually decreased. These results proved the specific identification and isolation of anti-EpCAM-MNs nanocomposite for MCF-7 and the high specificity of the PEC biosensor for MCF-7 detection. To probe the stability of the PEC biosensor, the photocurrent intensity was investigated under visible light with repeated "on-off" light irradiation cycles. The background photocurrent was almost stable after 12 on/off irradiation cycles (Fig. 5B). The relative standard deviation (RSD) of the photocurrent intensity was 0.43%. These results indicate good stability of the proposed PEC biosensor. In addition, the reproducibility of the PEC biosensor was studied with four parallel tests for 100 cell mL^{-1} of MCF-7. The RSD of the result was 1.6%, which indicates the good reproducibility of the PEC biosensing platform.

3.7. Detection of CTCs in whole blood samples

The applicability of the PEC biosensor for detecting CTCs in real samples was evaluated by recovery test of CTCs in whole blood samples. Various amounts of CTCs were spiked into whole blood samples, and the spiked CTCs were isolated and detected using the biosensor. The recovery results were between 95% to 110% with a relative standard deviation (RSD) ranging from 2.40% to 6.12% (Supporting Information, Table S2). Consequently, these data demonstrated that the biosensor could be used for highly efficient isolation and identification of CTCs in the complicated blood matrix.

4. Conclusions

In summary, a HCNT-based PEC biosensor was reported for efficient and sensitive CTCs detection. By integrating anti-EpCAM-MNs nanocomposite for enrichment as well as isolation of CTCs and Cu_2O-aptamer probe for amplifying the detection response, the PEC biosensor was successfully applied for detection of MCF-7 with a linear response range from 3 cell mL^{-1} to 3000 cell mL^{-1} and a low detection limit (1 cell mL^{-1}). The PEC biosensor shows good performance for detection of CTCs in whole blood samples, which may have potential applications in cancer diagnostics and therapeutics. Due to the utilization of aptamer, future work can be done by introducing various aptamer-related signal amplification strategies, such as hybrid chain reaction (HCR), rolling circle amplification, to further improve the detection sensitivity in future works.

Author contribution statement

Junjun Luo: Investigation, Writing- Original draft preparation
Dong Liang: Formal analysis, Data Curation
Dan Zhao: Validation
Minghui Yang: Conceptualization, Methodology, Writing - Review &

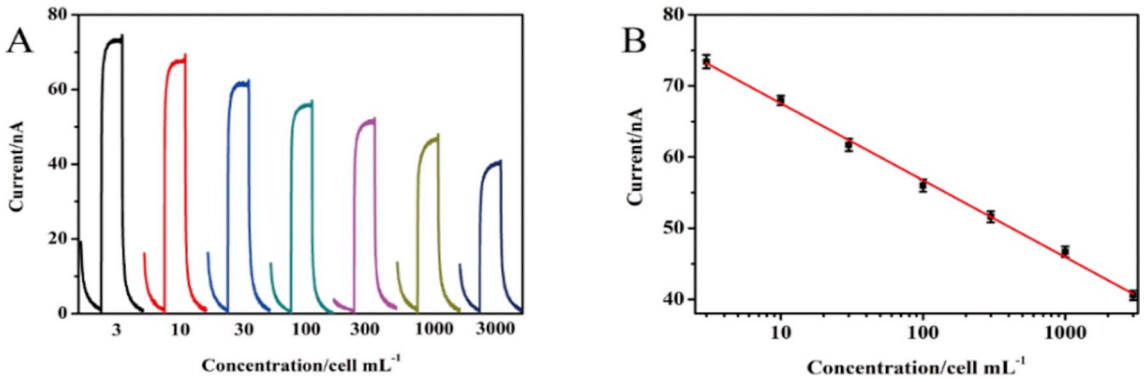

Fig. 4. (A) Photocurrent responses of the PEC biosensor toward MCF-7 cell at different concentrations: 3, 10, 30, 100, 300, 1000, 3000 cell mL^{-1}. (B) calibration curve of the PEC biosensor to different concentrations of MCF-7. Supporting electrolyte, 1 mM Na_2SO_4.

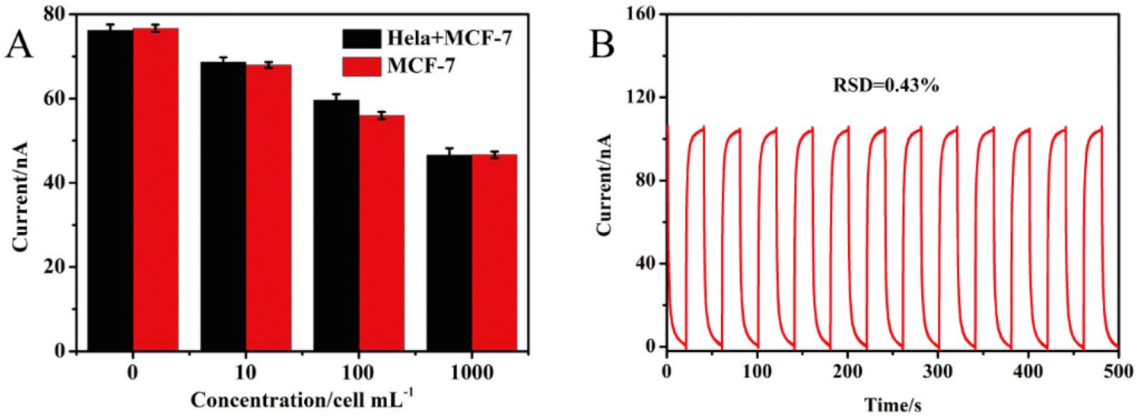

Fig. 5. (A) Comparison of the specific recognition of the PEC biosensor for HeLa cells and MCF-7 cells: various concentrations of MCF-7 cells (0, 10, 100, 1000 cells mL^{-1}) were mixed with 1000 cells mL^{-1} of HeLa. (B) Stability of the PEC biosensor under repeated light irradiation.

Editing, Supervision

Declaration of competing interest

The authors declare that they have no known competing financial interests or personal relationships that could have appeared to influence the work reported in this paper.

Acknowledgements

The authors thank the support of this work by the National Natural Science Foundation of China (Grant No.21575165).

Appendix A. Supplementary data

Supplementary data to this article can be found online at https://doi.org/10.1016/j.bios.2019.111976.

References

Asen, P., Shahrokhian, S., 2017. J. Phys. Chem. C 121, 6508–6519.
Fan, G.C., Zhu, H., Du, D., Zhang, J.R., Zhu, J.J., Lin, Y., 2016. Anal. Chem. 88, 3392–3399.
Ghamgosar, P., Rigoni, F., You, S., Dobryden, I., Kohan, M.G., Pellegrino, A.L., Concina, I., Almqvist, N., Malandrino, G., Vomiero, A., 2018. Nano Energy 51, 308–316.
Goyal, A., Reddy, A.L.M., Ajayan, P.M., 2011. Small 7, 1709–1713.
Guo, S., Deng, Z., Li, M., Jiang, B., Tian, C., Pan, Q., Fu, H., 2016. Angew. Chem. Int. Ed. 55, 1830–1834.
He, F., Wang, J., Yin, B.C., Ye, B.C., 2018. Anal. Chem. 90, 8072–8079.
Hu, X., Zhang, Y., Wang, B., Li, H., Dong, W., 2019. Appl. Catal. B Environ. 256, 117789.
Hu, Y., Hao, X., Cui, Z., Zhou, J., Chu, S., Wang, Y., Zou, Z., 2020. Appl. Catal. B Environ. 260, 118131.
Hua, X., Zhou, Z., Yuan, L., Liu, S., 2013. Anal. Chim. Acta 788, 135–140.
Huang, T., Jia, C.P., Jun, Y., Sun, W.J., Wang, W.T., Zhang, H.L., Cong, H., Jing, F.X., Mao, H.J., Jin, Q.H., Zhang, Z., Chen, Y.J., Li, G., Mao, G.X., Zhao, J.L., 2014. Biosens. Bioelectron. 51, 213–218.
Ji, Y., Liu, J., Liu, X., Yuen, M.M.F., Fu, X.Z., Yang, Y., Sun, R., Wong, C.P., 2017. Electrochim. Acta 248, 299–306.
Jiang, D., Du, X., Zhou, L., Li, H., Wang, K., 2017. Anal. Chem. 89, 4525–4531.
Kallatt, S., Nair, S., Majumdar, K., 2018. Small 14, 1702066.
Khan, R., Ahmad, R., Rai, P., Jang, L.W., Yun, J.H., Yu, Y.T., Hahn, Y.B., Lee, I.H., 2014. Sens. Actuators B Chem. 203, 471–476.
Kim, C., Cho, K.M., Al-Saggaf, A., Gereige, I., Jung, H.T., 2018. ACS Catal. 8, 4170–4177.
Li, C., Zhang, M., Zhang, Z., Tang, J., Zhang, B., 2019. Sens. Actuators B Chem. 297, 126759.
Li, L., Zheng, X., Huang, Y., Zhang, L., Cui, K., Zhang, Y., Yu, J., 2018a. Anal. Chem. 90, 13882–13890.
Li, R., Tu, W., Wang, H., Dai, Z., 2018b. Anal. Chem. 90, 9403–9409.
Li, X., Zhu, L., Zhou, Y., Yin, H., Ai, S., 2017a. Anal. Chem. 89, 2369–2376.
Li, Z., Pi, Y., Xu, D., Li, Y., Peng, W., Zhang, G., Zhang, F., Fan, X., 2017b. Appl. Catal. B Environ. 213, 1–8.
Lin, M., Chen, J.F., Lu, Y.T., Zhang, Y., Song, J., Hou, S., Ke, Z., Tseng, H.R., 2014. Acc. Chem. Res. 47, 2941–2950.
Liu, S., Lu, F., Jia, X., Cheng, F., Jiang, L.P., Zhu, J.J., 2011. CrystEngComm 13, 2425–2429.
Luo, J., Liang, D., Qiu, X., Yang, M., 2019. Anal. Bioanal. Chem. 411, 6889–6897.
Lv, J., Kong, C., Xu, Y., Yang, Z., Zhang, X., Yang, S., Meng, G., Bi, J., Li, J., Yang, S., 2017. Sens. Actuators B Chem. 248, 630–638.
Miao, P., Tang, Y., 2019. Anal. Chem. 91, 15187–15192.
Motaghi, H., Ziyaee, S., Mehrgardi, M.A., Kajani, A.A., Bordbar, A.K., 2018. Biosens. Bioelectron. 118, 217–223.
Musselman, K.P., Marin, A., Schmidt-Mende, L., MacManus-Driscoll, J.L., 2012. Adv. Funct. Mater. 22, 2202–2208.
Ouyang, J., Chen, M., Bao, W.J., Zhang, Q.W., Wang, K., Xia, X.H., 2015. Adv. Funct. Mater. 25, 6122–6130.
Peng, B., Tang, L., Zeng, G., Fang, S., Ouyang, X., Long, B., Zhou, Y., Deng, Y., Liu, Y., Wang, J., 2018. Biosens. Bioelectron. 121, 19–26.
Qiu, B., Li, Q., Shen, B., Xing, M., Zhang, J., 2016. Appl. Catal. B Environ. 183, 216–223.
Qiu, Z., Shu, J., Tang, D., 2018. Anal. Chem. 90, 1021–1028.
Shen, C., Liu, S., Li, X., Yang, M., 2019. Anal. Chem. 91, 11614–11619.
Shyamal, S., Maity, A., Satpati, A.K., Bhattacharya, C., 2019. Appl. Catal. B Environ. 246, 111–119.
Song, C., Zhao, Z., Sun, X., Zhou, Y., Wang, Y., Wang, D., 2019. Small 15, 1804268.
Tian, N., Xiao, K., Zhang, Y., Lu, X., Ye, L., Gao, P., Ma, T., Huang, H., 2019. Appl. Catal. B Environ. 253, 196–205.
Wang, K., Dong, X., Zhao, C., Qian, X., Xu, Y., 2015. Electrochim. Acta 152, 433–442.
Wang, T., Zhang, L., Wang, H., Yang, W., Fu, Y., Zhou, W., Yu, W., Xiang, K., Su, Z., Dai, S., Chai, L., 2013. ACS Appl. Mater. Interfaces 5, 12449–12459.
Wang, Z., Chen, M., Huang, Y., Shi, X., Zhang, Y., Huang, T., Cao, J., Ho, W., Lee, S.C., 2018. Appl. Catal. B Environ. 239, 352–361.
Wei, Y., Chang, X., Wang, T., Li, C., Gong, J., 2017. Small 13, 1702007.
Wen, C.Y., Wu, L.L., Zhang, Z.L., Liu, Y.L., Wei, S.Z., Hu, J., Tang, M., Sun, E.Z., Gong, Y. P., Yu, J., Pang, D.W., 2014. ACS Nano 8, 941–949.
Wu, L., Wang, J., Ren, J., Qu, X., 2014. Adv. Funct. Mater. 24, 2727–2733.
Wu, Z., Cheung, G., Wang, J., Zhao, Z., Osterloh, F.E., 2018. Chem. Commun. 54, 9023–9026.
Xu, Y.T., Guo, Y., Li, C., Zhou, X.Y., Tucker, M.C., Fu, X.Z., Sun, R., Wong, C.P., 2015. Nano Energy 11, 38–47.
Yan, X., Song, Y., Liu, J., Zhou, N., Zhang, C., He, L., Zhang, Z., Liu, Z., 2019. Biosens. Bioelectron. 126, 734–742.
Yang, R., Zou, K., Li, Y., Meng, L., Zhang, X., Chen, J., 2018a. Anal. Chem. 90, 9480–9486.
Yang, Y., Fu, Y., Su, H., Mao, L., Chen, M., 2018b. Biosens. Bioelectron. 122, 175–182.
Zeng, Z., Yan, Y., Chen, J., Zan, P., Tian, Q., Chen, P., 2019. Adv. Funct. Mater. 29, 1806500.
Zhang, J., Liu, J., Peng, Q., Wang, X., Li, Y., 2006. Chem. Mater. 18, 867–871.
Zheng, F., Cheng, Y., Wang, J., Lu, J., Zhang, B., Zhao, Y., Gu, Z., 2014a. Adv. Mater. 26, 7333–7338.
Zheng, T., Zhang, Q., Feng, S., Zhu, J.J., Wang, Q., Wang, H., 2014b. J. Am. Chem. Soc. 136, 2288–2291.